Journal of Materials Science & Technology 71 (2021) 31–43

Contents lists available at ScienceDirect

Journal of Materials Science & Technology

journal homepage: www.jmst.org

Research Article

Polyetheretherketone with citrate potentiated influx of copper boosts osteogenesis, angiogenesis, and bacteria-triggered antibacterial abilities

Jianglong Yan[a], Dandan Xia[b], Pan Xiong[a,d], Yangyang Li[a], Wenhao Zhou[a], Qiyao Li[c], Pei Wang[a], Yufeng Zheng[b,*], Yan Cheng[a,*]

[a] Academy for Advanced Interdisciplinary Studies, Peking University, Beijing 100871, China
[b] Department of Materials Science and Engineering, College of Engineering, Peking University, Beijing 100871, China
[c] Department of Biomedical Engineering, Materials Research Institute, Huck Institutes of the Life Sciences, The Pennsylvania State University, University Park, PA 16802, USA
[d] The Science and Technology Bureau of Chengdu, Chengdu Administration of Foreign Experts Affairs, Chengdu 610042, China

ARTICLE INFO

Article history:
Received 30 May 2020
Received in revised form 30 June 2020
Accepted 9 July 2020
Available online 9 September 2020

Keywords:
Citrate
Copper
Potentiated influx
Bone regeneration
Angiogenesis
Bacteria-triggered coating

ABSTRACT

A well designed coating for polyetheretherketone (PEEK) implants can provide enough support to overcome crucial medical challenges, which are insufficient osseointegration and high rate of infection. Herein, we utilize the co-deposition of polydopamine (PDA) and copper-citrate nanoclusters to construct a pH-responsive coating on porous PEEK for synergistic bone regeneration, vascular formation and anti-infection. Specifically, this PDA coating released high dose of copper and citrate at lower pH value, which increased intracellular copper content, boosted production of reactive oxygen species and severe damage of protein, leading to killing of 93 % planktonic bacterial and eradication of adherent bacteria. At pH of 7.4, the release of copper and citrate were in a slow and sustained behavior, synergistically enhanced vascular formation potential and osteodiffereration of Ad-MSC *in vitro*. After implanted in rabbit tibia for 6 and 12 weeks, the micro-CT evaluation and histological analysis consistently highlighted the ability of this PDA coating to increase new bone formation adjacent to coated PEEK implant and enhance bone-implant interfacial integration. These results were proven to be related to the synergistic effect that citrate facilitated a 2-fold influx of copper into cells, which not only enhanced the bacteria-killing ability but also encouraged bone regeneration of implants. This present work provides an effective method to control infections while promoting osseointegration simultaneously, which will show tremendous clinical application and can be a solution to current challenges facing orthopedics.

1. Introduction

Polyetheretherketone (PEEK) has attracted increasing attention as an orthopedic implant because of its excellent chemical resistance, natural radiolucency, magnetic resonance imaging compatibility, wear resistance, and most important, its similar mechanical properties to cortical bone [1]. However, its chemical and biological inertness, which usually associates with implant-associated infection and insufficient osseointegration, tends to limit its application. Therefore, it appears necessary to endow antibacterial and osteogenic ability to PEEK.

Many strategies have been applied to combatting with the implant-associated infection as it may lead to secondary surgery, which would increase not only patient suffering but also health costs. These strategies mainly include the coating of some antifouling polymers to repel bacteria and the immobilization/release of organic/inorganic bactericides to kill bacteria [2–6]. Nevertheless, the repelling coatings will inevitably become contaminated by bacteria and the bactericidal coatings are hindered by the rising problem of multidrug-resistant (MDR) bacteria. Therefore, it turns to be necessary to explore a new strategy to kill bacteria efficiently while prevent the development of MDR. Our previous study utilized the synergistic bactericidal effect of silver and gentamicin sulfate to eliminate bacteria and prevent the development of MDR

* Corresponding author.
E-mail addresses: yfzheng@pku.edu.cn (Y. Zheng), chengyan@pku.edu.cn (Y. Cheng).

https://doi.org/10.1016/j.jmst.2020.08.048
1005-0302/

[7]. However, the utilization of silver caused contradiction between antibacterial ability and biocompatibility as its antibacterial ability associates with cytotoxicity, which would lead to difficulties in balancing antibacterial and biocompatibility. Hence, the key is to find a strategy that can balance antibacterial and biocompatibility of implant, which means inhibiting bacteria while promoting osteodifferentiation of bone cells.

Copper has been reported to possess osteogenic and antimicrobial abilities, and it has been used in biomaterials to promote bone formation and prevent infection [8–10]. However, a high concentration of Cu^{2+} (256 μg/mL) is needed to kill bacteria while a relative low concentration of Cu^{2+} (0.1 mM/6.4 μg/mL) will be enough for osteogenesis [11,12]. Thus, we combined copper nanoclusters (CuNs) with citrate which also has been widely used in biomaterial to facilitate bone regeneration and kill bacteria [13]. In addition, citrate kill bacteria *via* traversing cell membranes and causing damage to particular enzymes [14], while copper kill bacteria through disrupting cell membranes, elevating production of reactive oxygen species (ROS), and binding to protein or DNA [15]. It is clear that copper and citrate share different pathways to kill bacteria and it is known that synergistic antibacterial effect can come from bactericides cocktail attacking bacteria from different fronts. In this way, bacteria can be killed at relative low concentration of Cu^{2+}, which would be beneficial to the balance between biocompatibility and bactericidal activity. To achieve the switch of PEEK implant's bio-function between osteogenesis and antibacterial, we planned to manipulate the release of Cu^{2+} under different situations through the utilization of pH-responsive controlled release property. It can help to achieve the low concentration and sustained release of copper-citrate nanoclusters under physiological conditions, which is expected to promote the bone formation; and achieve high concentration release of copper-citrate nanoclusters only if bacteria are present. To achieve this on-demand release of copper-citrate nanoclusters, polydopamine (PDA) was chosen. It is an important platform for surface functionality and stabilization agent in the fabrication of diverse organic-inorganic materials, most importantly it possesses excellent biocompatibility and pH responsive charge variation and degradation [16].

However, the two performances of osteogenesis and bacteria-killing may not be able to guarantee both rapid bone regeneration and sufficient early stability of implants. Impaired bone healing is also associated with a reduction of vascular supply, which would lead to compromised nutrient availability at the site of injury. It highlights the importance of functional angiogenic response to successful implantation [17]. Actually, active angiogenesis is a prerequisite step to achieve the successes of bone integration as blood vessels transport oxygen, nutrients and factors to the site of bone fracture [18]. Thus, it appears necessary to endow angiogenic ability to implants. The chosen copper has been proved to be able to promote angiogenesis by artificially mimicking hypoxia through stabilizing the structure of hypoxia-inducible factor (HIF-1α), in turn stimulating the secretion of VEGF [19], which plays an important role in the recruitment and differentiation of cells and in blood vessel formation [20,21]. In addition, citrate also has been reported to induce angiogenesis [22]. Hence, implants with copper-citrate nanoclusters are expected to facilitate angiogenesis.

The cross-talk between endothelial cells (ECs) and osteoblastic cells (OBs) also can affect bone repairing, as blood vessel growth and osteogenesis are coupled during bone remodeling [23]. Therefore, it would be important for us to understand the influences of implants on the crosstalk of ECs and OBs. For this purpose, a coculture system with adipose-derived mesenchymal stem cells (Ad-MSCs) and human umbilical vein endothelial cells (HUVECs) was designed, and effects of implants on the crosstalk of cells would be evaluated by their osteogenesis and angiogenesis performance.

In this study, copper-citrate nanoclusters were co-deposited with dopamine upon the porous surface of PEEK implants, aimed to promote implant's osteogenesis, angiogenesis and antibacterial ability. In addition, the effects of implant on the communication between Ad-MSCs and HUVECs was investigated and the mechanism underlying the enhanced pH-responsive bacteria-killing effect was partially revealed.

2. Materials and methods

2.1. Preparation of copper nanoclusters

Two different kinds of copper nanoclusters were prepared, one is dopamine (DA) stabilized copper nanoclusters and another is capped by citrate. Briefly, $CuSO_4{\cdot}5H_2O$ (0.5 *g*) and reducing agent L-ascorbic acid (1 *g*) were dissolved into 90 mL deionized (DI) water, followed by the adding of capping agents DA (0.612 *g*) and trisodium citrate (1.2 *g*) into this solution respectively. Then the two mixtures were kept at 80 °C under magnetic stirring until dark solutions were obtained. The resulting dispersions were centrifuged at 8500 rpm for 20 min followed by the collection of DA capped copper nanoclusters and citrate capped copper nanoclusters.

2.2. Preparation of porous PEEK with PDA assisted deposition of copper nanoclusters

Medical grade PEEK (KetaSpire, Solvay, Belgium) materials were used in this study. Samples were machined into disk shape with dimensions of $\Phi 15 \times 1.5$ mm^3 for *in vitro* studies, and rod samples with 2 mm in diameter and 6 mm in length were employed in animal evaluation. All the samples were mechanically polished up to 2000 grits and ultrasonically washed in acetone, ethanol, and deionized water sequentially.

The surface modification process is illustrated in Fig. 1. PEEK was treated with sulfuric acid (95–98 wt%, Aldrich Chemical Corp) under supersonically stirred at room temperature for 5 min. Subsequently, samples were ultrasonically rinsed in DI water before hydrothermal treatment at 100 °C for 4 h (labeled as SP). After that, copper nanoclusters were incorporated onto the surface of SP under the aid of PDA. In brief, SP samples were immersed into Tris–HCl buffer (10 mM, pH = 8.5, Sigma) containing 2 mg/mL dopamine hydrochloride (Aladdin) before the addition of copper nanoclusters and were kept in a shaker in darkness at 37 °C for 12 h. The samples incorporated with DA capped copper nanoclusters were labeled as DCuN while the samples incorporated with citrate capped copper nanoclusters were labeled as CCuN.

2.3. Surface characterization

Field-emission high resolution transmission electron microscope (FE-TEM, JEM-2100 F, JEOL, Japan) was used to analyze the copper nanoclusters. The morphology and microstructure of samples with different coatings were observed by Field-emission scanning electron microscope (FE-SEM, S-4800, Hitachi, Japan) under voltage of 5 kV and working distance of 8 mm. X-ray photoelectron spectroscopy (XPS, Kratos, UK) were used for compositional analysis. SL200B contact angle system (Kino, USA) were employed to determine the surface hydrophilicity,and deionized water was used.

2.4. Cu^{2+} release into phosphate buffer solution (PBS)

To investigate the release behavior of Cu^{2+}, samples (DCuN and CCuN) were placed into 24-well plates, and 2 mL PBS with different pH (pH = 7.4, 5.0) was added into each well. Then samples were placed into incubator at 37 °C for 28 d. At predetermined time

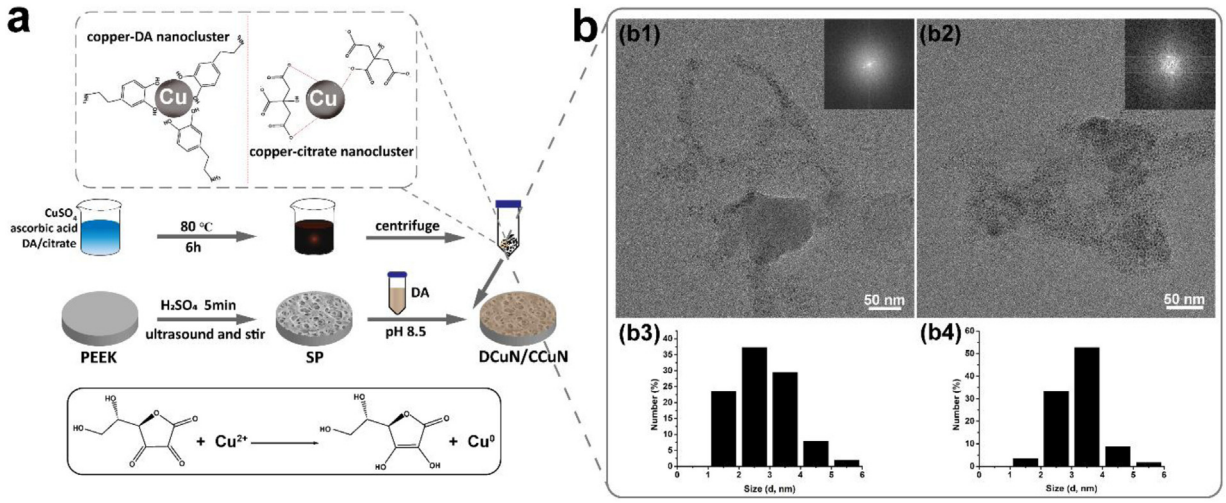

Fig. 1. (a) Scheme illustration of surface functionalization of PEEK. TEM images of (b1) DA capped CuNs and (b2) citrate capped CuNs with FFT images on the top right corner, and size distribution of (b3) DA capped CuNs and (b4) citrate capped CuNs analyzed with ImageJ software.

points, the solution was collected and refilled with fresh PBS. The amount of released Cu^{2+} was determined by inductively coupled plasma-mass spectrometry (ICP-MS, Agilent 7700, USA).

To further verify the pH controlled release of Cu^{2+}, samples (DCuN and CCuN) were immersed into 2 mL PBS with pH of 7.4 in the first seven days and then changed pH value to 5.0 in the next seven days. The solution was collected and refilled at predetermined time points and the concentration of Cu^{2+} was analyzed by ICP-MS.

2.5. Bacteria culture and inoculation

Gram-negative *Escherichia coli* (*E.coli*, ATCC 25922) was incubated in Luria-Bertani (LB) broth at 37 °C overnight, then it was diluted with LB medium to a concentration of 1.0×10^6 colony forming units (CFU) mL^{-1}. This bacteria solution were incubated with specimens for different time periods.

2.6. Antibacterial rate

A pH-responsive antibacterial ability was designed to PDA based coating. To evaluate its effectiveness, samples were incubated with bacteria at different pH values. Specifically, the antibacterial rates were evaluated by incubating samples with 1 mL bacteria suspension in LB medium with different pH value (pH 7.4 and 5.0) at 37 °C for 6 h. Then standard serial dilution and plate-counting were used to quantify the active bacteria in the suspension, and the antibacterial rate was calculated by the following formula:

$$\text{Antibacterial rate } (\%) = \frac{A - B}{A} * 100\%$$

where A is the average number of bacteria colonies on the control group (PEEK samples, CFU mL^{-1}) and B is the average number of bacteria colonies on the experimental groups (CFU mL^{-1}).

2.7. Microbial viability assay

The viability of bacteria adhered to the samples was assessed by the Microbial Viability Assay Kit-WST (Dojindo, Kumamoto, Japan). After incubated with bacteria in LB medium with pH 5.0, samples were taken out and washed with PBS before the addition of LB medium which contains 5% of WST-8 reagent. They were kept at 37 °C for 2 h, then the absorbance was read at the wavelength of 450 nm by a microplate reader ((Bio-RAD, USA).

2.8. SEM observation of bacteria morphology

The bacteria suspension (LB, pH 5.0) was introduced onto the samples and incubated for 6 h for anti-attachment assessment and 7 d for anti-biofilm assessment. Afterwards, samples were rinsed in PBS, then fixed with 2.5 % glutaraldehyde and graded ethanol. Finally, the adherent bacteria were observed by SEM.

2.9. Membrane permeability measurements

Propidium iodide (PI) (Invitrogen, USA), which can only be uptake by cells with compromised membrane, was used to monitor membrane permeability. The bacterial cells were incubated with samples in LB medium with pH 5.0 for 6 h, then bacteria were collected after centrifugation of bacterial suspension and refilled with PI (3 μL mL^{-1}) in 0.85 % NaCl. This mixture was mixed thoroughly and incubated at room temperature under dark condition for 15 min. The fluorescence intensity was measured in a 96-well plate by a microplate reader (SPECTRAMAX M5, MD, China) with excitation/emission at 488/630 nm, and the obtained intensities were normalized to that of PEEK group.

The protein concentration in the bacteria suspension was determined by the Pierce BCA Protein Assay Kit (Thermo Scientific, USA) after bacteria incubating with samples in PBS with pH 5.0 for 6 h.

2.10. Intracellular production of reactive oxygen species (ROS)

DCFH-DA dye was used to measure the intracellular ROS generation. It was added into solution (final concentration 10 μM) for 30 min after bacteria cultured with samples for 6 h. Bacteria were collected by centrifugation and then suspended in the same volume of PBS. The fluorescence intensity of this solution was detected by a microplate reader in fluorescence mode with excitation and emission at 488 nm and 525 nm respectively.

2.11. Measurement of Cu uptake

The bacteria were treated with samples in LB medium at pH 5.0 for 6 h. A 100 μL aliquot of suspension was plated on agar plates for bacteria counting and the rest of bacteria suspension was washed in DI water with 1 mM EDTA before washed three times in DI water. After that, the collected bacteria were digested in HNO_3 (GR, Beijing Chemical Reagent Co., Ltd., China) overnight and heated at 80 °C for 30 min. This solution was diluted with DI water and analyses were

performed on ICP-MS. The measured Cu content was normalized to the number of bacteria.

2.12. Cell culture

Ad-MSCs and HUVECs were employed and cultured in α-MEM and ECM, respectively. Ad-MSCs at passages of 3–5 and HUVECs at passages of 3–5 were used in this study, and seeding densities for Ad-MSCs and HUVECs at 20,000 and 40,000 cells/cm^2 respectively were employed for all of monoculture and coculture. The medium for osteogenic assays was a cocktail of α-MEM with osteogenic factors (ascorbic acid, dexamethasone and β-glycerophosphate) and for coculture system was the 1:1 mixture of ECM and α-MEM.

2.13. Cell adhesion and proliferation of Ad-MSCs and HUVECs

To observe cell adhesion, cells were incubated with specimens in a 24-well plate for 12 h, then 2.5 % (v/v) glutaraldehyde was utilized to fix cells at 4 °C overnight and then dehydrated in graded ethanol before SEM observation. For confocal laser scanning microscope (CLSM) observation, 4% paraformaldehyde (PFA) was used to fix Ad-MSCs and then 0.1 % Triton X-100 was used to permeabilize cells before double stained with fluorescein (FITC)-conjugated phalloidin (5 μg mL^{-1}) and DAPI (2 μg mL^{-1}).

To assess cell proliferation, the MTT cell proliferation assay kit (Beyotime, China) was employed after samples incubated with Ad-MSCs for 1, 3 and 5 d or incubated with HUVECs for 1 and 3 d. In brief, the culture medium with 10 % of MTT was added and incubated with samples at 37 °C for 4 h, then the medium was discarded and refilled with dimethyl sulfoxide (DMSO) to solubilize the formed formazan, and microplate reader was used to measure the absorbance of this formazan solution at wavelength of 570 nm.

2.14. Vascularization and osteogenic differentiation of mono-cultured and co-cultured cells

To evaluate the vascularization of cells, the released NO was quantified through the utilizing of griess reagent system (Promega, USA) after cell cultured with samples in monoculture or coculture system for 24 h. Briefly, 50 μL of lysed cell suspension incubated with the reagent solution, and finally a purple/magenta color appeared. The absorbance of this solution was measured by a microplate reader at 520 nm, and the nitrite content was calculated based on a standard curve constructed with sodium nitrite.

To determine the osteogenic differentiation of Ad-MSCs, they were seeded on samples for monoculture or seeded with HUVECs on samples for coculture. Afterwards, qualitative and quantitative of alkaline phosphatase (ALP) expression were determined with BCIP/NBT alkaline phosphatase color development kit (Beyotime, China) and alkaline phosphatase assay kit (Beyotime, China) after incubation for 7 d. After incubation for 14 d, samples were stained with 0.1 % solution of Sirius Red (Sigma, USA) in saturated picric acid for imaging and the absorbance of the destaining solution (0.2 M NaOH/methanol 1:1) which incubated with stained samples was measured at 570 nm by microplate reader. The extracellular matrix (ECM) mineralization performance was studies after incubation for 21 d, qualitative analysis was performed by staining with Alizarin Red S (ARS, Sigma; 2%, pH = 4.3) at 4 °C, and quantitative analysis was achieved by measuring the absorbance of calcium dissolving solution (10 % cetylpyridinium chloride).

2.15. Gene expression analysis

The expression of angiogenesis related genes were analyzed by the real-time reverse-transcriptase polymerase chain reaction (RT-PCR). After HUVECs cultured with samples for 3 d, total RNA was extracted with TRIzol reagent (TIANGEN BIOTECH, China) and converted to cDNA using a RevertAid First Strand cDNA Synthesis Kit (Thermo Fisher, USA). Then RT-PCR was carried out using SYBR Green (Roche, USA) on an ABI 7500 RT-PCR machine (Applied Biosystems, USA). The primers used in this study are listed in Table S**1**. The relative mRNA expression level of genes were normalized with the housekeeping gene18S rRNA and determined by the cycle threshold (Ct) value according to the $\Delta\Delta$Ct method.

2.16. Surgery

This animal surgery was approved by Ethics Committee of Peking University Health Science Center, and the surgical procedures were performed in accordance with Experimental Animal Ethics Branch (LA2019019). In detail, the rabbit (New Zealand White) tibia model was used to estimate new bone formation adjacent to and osseointegration of implants. Six 3-month-old rabbits were randomly assigned to different implants. Before implantation, pentobarbital sodium (30 mg/kg) was injected into marginal ear veins of rabbits for anesthesia. Then three holes with diameter of 2 mm and depth of 6 mm were drilled at both the left and right tibia of rabbits, subsequently samples was inserted into these holes. After operation, the rabbits were housed in a separate cages. At 6 or 12 weeks, rabbits were sacrificed and rabbit tibias were removed and then fixed in 10 % neutral formalin buffer before micro-CT analysis and histological observation.

2.17. Micro computed tomography (micro-CT) analysis

Micro-CT (Inveon MM CT; Siemens, Germany) was used to analysis the newly formed bone around the implants. Scanning was performed at 80 kV and images (2D and 3D) were reconstructed by Inveon Research Workplace software (Siemens, Germany). Besides, the bone mineral density (BMD) and bone volume over total volume (BV/TV) was calculated.

2.18. Histological evaluation

For histological analysis, the fixed implants were rinsed in water, dehydrated in graded ethanol, and embedded in methylmethacrylate. Afterwards, the embedded implants were cut into sections with thickness of 200 μm and kept grinding to thickness of 20 μm. These sections were observed by SEM or observed with optical microscope after stained with methylene blue and acid fuchsine.

2.19. Statistical analysis

At least three samples were prepared for each data point, and corresponding results were presented as mean ± standard deviations. Statistically significant difference (P) between groups was measured by one-way analysis of variance (ANOVA), and P values < 0.05 were considered to be statistically significant.

3. Results and discussion

3.1. Preparation and characterization of copper-citrate nanoclusters contained porous surface

To achieve successful implantation without the emergence of MDR, a triple-function system was constructed on the surface of PEEK (Fig. 1a). First, a three dimensional (3D) porous structure was fabricated onto the surface of PEEK (Fig. 2a) as it is beneficial to the ossification [24]. Then the produced copper-citrate nanoclusters (production mechanism and proposed structure displayed in Fig. 1a) were introduced through the co-deposition with PDA, while copper-DA nanoclusters were deposited on SP surface as a control

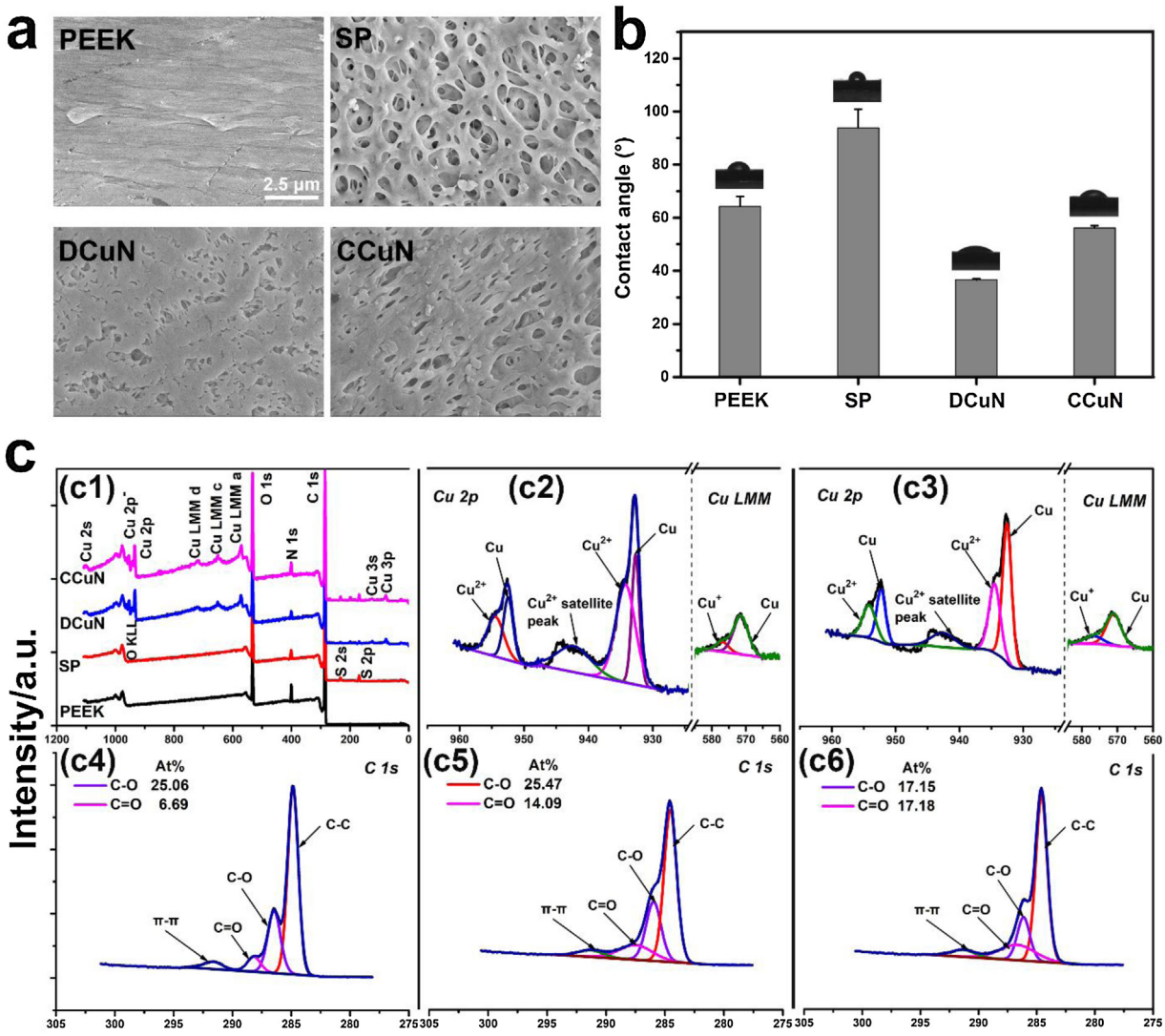

Fig. 2. (a) Surface morphology and (b) contact angle of different samples. Chemical composition of coatings: (c1) Survey spectra of XPS, and high resolution XPS spectra of (c2) Cu 2p from DCuN, (c3) Cu 2p from CCuN, (c4) C 1s from SP, (c5) C 1s from DCuN, and (c6) C 1s from CCuN.

group which contain CuNs and PDA layer without the presence of citrate. After the deposition procedure, a thick layer appeared on the surface of DCuN and CCuN samples. This layer on the surface of DCuN sample decreased the contact angle from 94° to 37° (Fig. 2b) and increased the percent of C=O compared to CO— (Fig. 2c4, c5). These correspond to the features of PDA and validate the existence of it [25,26]. The existence of PDA can control the leaked amount of copper, so as to control the switch of implants biological functions between osteogenesis and bacteria-killing. Copper was detected on the surface of DCuN and CCuN samples and displayed in the survey spectra of XPS (Fig. 2c1). The spherical shape and homogeneously distribution of both copper-DA and copper-citrate nanoclusters (Fig. 1b1, b2) with around 2∼3 nm in diameter (Fig. 1b3, b4) were preliminarily analyzed by TEM. Furthermore, the TEM images with higher magnification were presented as Fig. S1, which clearly revealed the size of nanoclusters. Additionally, the fast Fourier transform (FFT) images disclosed that the *d*-spacing was 2.1 Å for both copper-DA and copper-citrate nanoclusters, which indicates the formation of metallic copper. Further investigation on the introduced CuNs was conducted by XPS, and the high resolution Cu 2p and Cu LMM spectra of DCuN and CCuN samples indicate that Cu^0 is the dominant component of CuNs while Cu^{2+} and Cu^+ also exist (Fig. 2c2, c3). The fact that most of the copper content was in the state of Cu^0 reveals that copper nanoclusters would be a reservoir of Cu^{2+} and slow down the release rate of it. This would help to maintain Cu^{2+} in a concentration that is beneficial to bone regeneration and vessel formation. The existence of citrate in CCuN sample was supported by the increased ration of C=O/C-O from 0.55 of DCuN sample to 1.0 of CCuN sample, as there are higher ration of C=O/C-O in citrate and oxidized citrate than PDA (Fig. 1a). The existence of citrate was expected to synergize with copper to promote bone regeneration and antibacterial ability.

The pH-responsive release behavior was designed as a characteristic of this coating, and it was tested by immersing samples into solution with different pH values for varying time period. The release profiles of Cu^{2+} were measured and displayed in Fig. 3a. It is noteworthy that the release profile of Cu^{2+} from DCuN and CCuN samples were almost the same at different pH condition. The release amount of Cu^{2+} increased rapidly during the first week at pH 5.0 and reached at 9 μg, then the release amount of Cu^{2+} progressively increased to 10 μg after 28 d. At physiological environment, Cu^{2+} leaked into PBS at relative slow rate and gradually increased to 0.9 μg after immersion for 28 d. On the other hand, Fig. 3b displayed a pH responsive release behavior which was a slow release of Cu^{2+} during the first 7 d at pH 7.4 and a dramatically enhanced release rate instantly after exposure to PBS at pH 5.0.

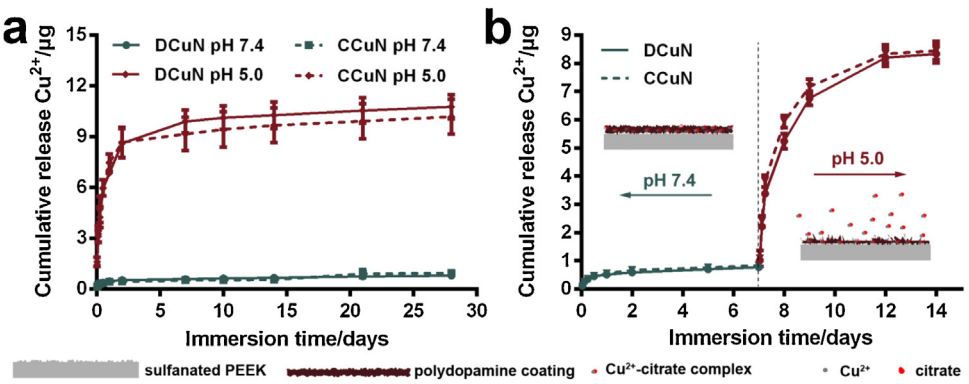

Fig. 3. (a) The cumulative release profile of copper at different pH condition, and (b) pH controlled release of copper from DCuN and CCuN samples.

Collectively, these results clearly shows that both DCuN and CCuN samples achieve pH responsive release of Cu^{2+}. PDA plays a key role in the pH-responsive release of copper. After deposition, the majority of CuNs are entrapped within the PDA layer and only a small amount of them are deposited on the surface of PDA membrane. When exposed to physiological pH (pH = 7.4), the structure of PDA is very stable and only these CuNs on the surface of PDA membrane release into PBS solution. This low amount of copper would benefit to ossification and vascularization. As environment pH decreases, amino groups in PDA are protonated, leading to the weakened or broken of PDA internal interaction [27], eventually results in the degradation of PDA membrane and fast release of copper (Fig. 3b). In addition, the decrease of pH accelerates oxygen dependent dissolution of Cu^{2+} from CuNs. These two factors contributes to the faster and larger amount release of copper under lower pH condition. This pH-responsive feature of coatings can control the concentration of Cu^{2+}, so as to promote new bone formation and vascular formation at physiological environment and enhance bactericidal effect as pH decrease. On the other hand, bacteria can metabolically acidify their local environment [28], indicating that the emergence of bacteria can trigger the release of copper. It means that this coating deliver bacteria-killing agents when and where bacteria appear, achieving bacteria-triggered self-defensive ability.

3.2. *In vitro antibacterial evaluation*

Once bacterial infection occurred, it is difficult to treat and may lead to failure of medical device implantation, not to mention the appearance of biofilm, which notoriously resists killing by host defense mechanisms and antibiotics [29]. Therefore, implants that can resist bacterial attachment and prevent biofilm formation would guarantee the success of implantation. Actually, this was one of the properties designed to the implant. As a proof-of-concept, *E.coli* was chosen to test the antibacterial ability of copper based-coatings as *E.coli* is one of the sources of implant infection and it can adapt to copper toxicity [30,31]. Most importantly, *E.coli* are resistant to external pH variation, minimizing the effect of pH variation on the growth of bacteria [32]. Specifically, samples were treated with *E.coli* in LB medium with different pH value (pH 7.4 and 5.0), and their antibacterial abilities were evaluated. At pH 7.4, the number of viable bacteria in the medium (Fig. S**2**) and the activity of adherent bacteria on the surface of samples were decreased after treated with CCuN samples (Fig. 4b). This showed the inhibition effect of CCuN samples on the activity of bacteria at physiological environment. At pH 5.0, the number of viable bacteria in the suspension of PEEK group was less than that at pH 7.4, which indicates lower pH could inhibit the activity of bacteria. However, the number of viable bacteria in the suspension at pH 5.0 was much lower than that at pH 7.4 for DCuN and CCuN groups. The antibacterial rates of DCuN and CCuN samples at pH 5.0 were 52 % and 93 %, respectively; while those at pH 7.4 were only 24 % and 42 %, respectively (Fig. 4a). The activities of adherent bacteria and the SEM images of adherent bacteria also revealed that much fewer bacteria adhered on the surface of DCuN and CCuN samples at pH 5.0 (Fig. 4b, g). These results prove that DCuN and CCuN samples have been equipped with bacteria-triggered self-defensive ability as the metabolism of bacteria can acidify the local environment, and that ability is originated from increased release of copper under lower pH environment.

At pH 5.0, both DCuN and CCuN samples increased the release amount of copper, which were almost at the same level. However, there were differences between the antibacterial abilities of DCuN and CCuN samples. 93 % of bacteria were killed in the suspension of CCuN group while 52 % of bacteria were killed in the suspension of DCuN group. Also, it was barely to find any bacteria on the surface of CCuN samples while there were bacteria scattered on the surface of DCuN samples, and the data of the microbial activity in accordance with these results. Furthermore, the long-term antibacterial ability was assessed (Fig. 4h). After cultured for 7 d, biofilm formed on the surface of PEEK sample. On the contrary, there were just a few bacteria littering on the surface of CCuN samples, and the majority of bacteria were with distorted or even broken structure while bacteria on the surface of DCuN presented a smoother and intact membrane. These indicate that CCuN samples possess better antibacterial ability than DCuN samples. This phenomenon was firstly considered associated with the differences in the released amount of copper and the structure of Cu^{2+}-DA and Cu^{2+}-citrate complexes. However, there were no difference in the release behavior of copper from DCuN and CCuN samples, and the release amount were nearly the same or even lesser from CCuN samples than from DCuN samples. It excludes the influence of the released amount of copper on this difference and suggests that the differences of structure between Cu^{2+}-DA and Cu^{2+}-citrate complexes should be the key. As exhibited in Fig. 1a, copper-citrate nanoclusters are complexes of copper nanoclusters and citrate, the liberated Cu^{2+} would form complex with citrate due to the electrostatic interaction. It has been reported that organic acid could potentiate the influx of metals into bacteria, which is independent of pH [33]. Meanwhile, citrate is capable to traverse bacterial membrane and lead to bacteria death [14]. Concluded from that, we reasoned Cu^{2+}-citrate complexes would be more likely to enter bacteria than Cu^{2+}-DA complexes, resulting in a locally high concentration of copper within bacteria. The localized copper could increase intracellular reactive oxygen species (ROS) production which would be detrimental to bacteria by disturbing different metabolisms of bacteria. To verify this hypothesis, experiments were carried out. As depicted in Fig. 4c, d, the relative PI intensity and the protein leakage in CCuN group were higher than those in DCuN group. Fig. 4f demonstrated that

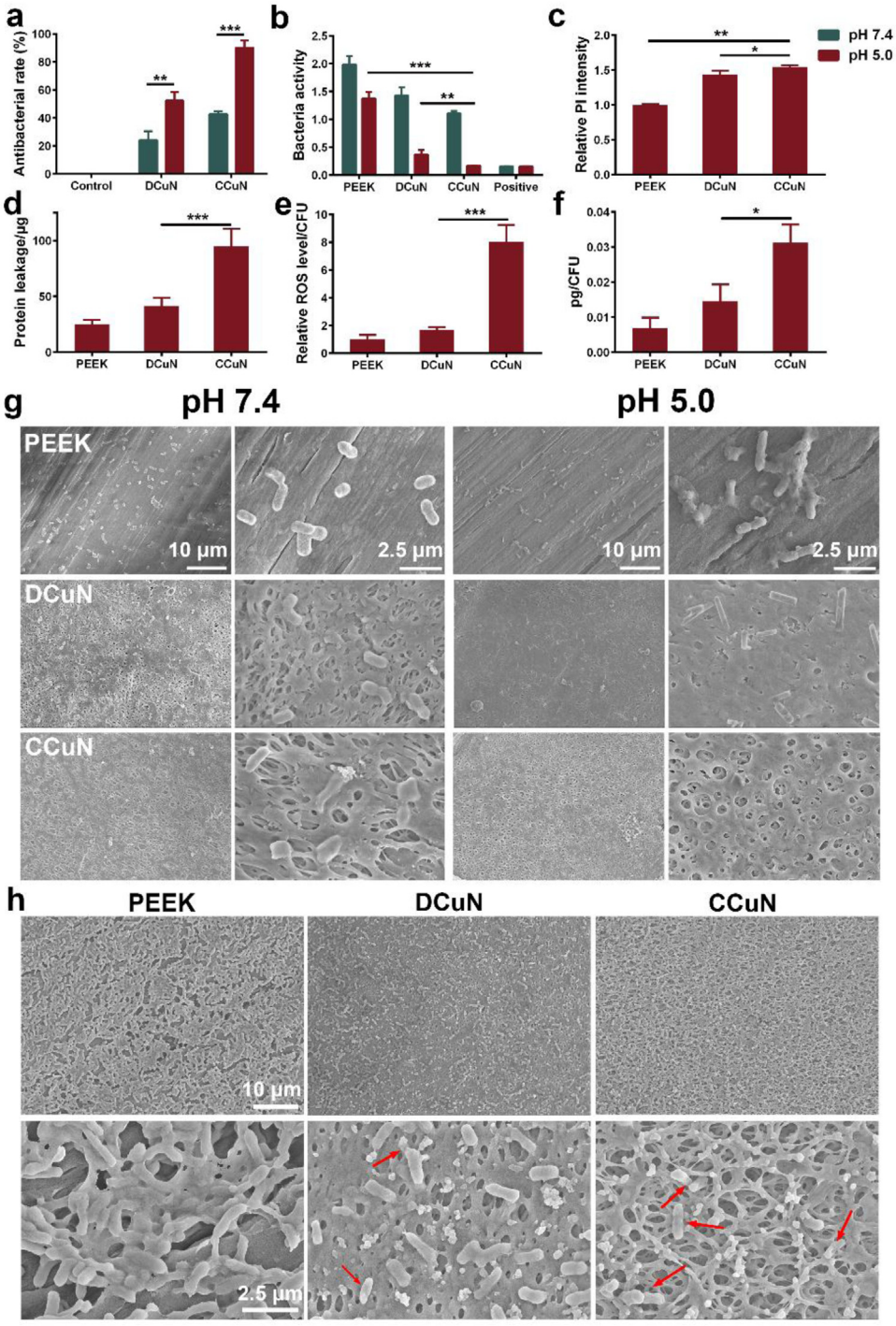

Fig. 4. Antibacterial evaluation: (a) antibacterial rate of different samples and (b) activity of bacteria adhered to different samples after treated with *E. coli* at different pH value for 6 h. After treated with different samples at pH 5.0 for 6 h, (c) relative PI intensity, (d) protein leakage, (e) relative ROS level, and (f) concentration of copper per bacteria. SEM observation of bacteria morphology after cultured with samples for (g) 6 h and (h) 7 d. $^{*}P < 0.05$; $^{**}P < 0.01$; $^{***}P < 0.001$.

CCuN treatment facilitated the influx of copper into bacteria compared with DCuN treatment while much higher ROS production in CCuN group than in DCuN group was illustrated in Fig. 4e. These results perfectly confirmed our hypothesis and a more detailed bacterial killing mechanism could be deduced (Fig. 5). The Cu^{2+}-citrate complexes could be regarded as a kind of nano-antibiotic, and they cause greater damage to bacterial membrane than copper or citrate alone. This damage can engender protein leakage, leading to bacterial death. Meanwhile, it would enable more copper flow into bacteria and bring about localized high concentration of copper within bacteria. This localized high concentration of copper could elevate intracellular ROS production through catalyzing Fenton chemistry and hydroxyl radical formation [34,35], and the elevated ROS would lead to DNA damage and inhibition of particular enzyme activities, causing detrimental effects to bacteria [36]. On the other hand, the localized high concentration of copper itself could bind to some particular proteins, thus abolishing enzyme activity and disturbing bacteria metabolisms, triggering bacterial death [15,37].

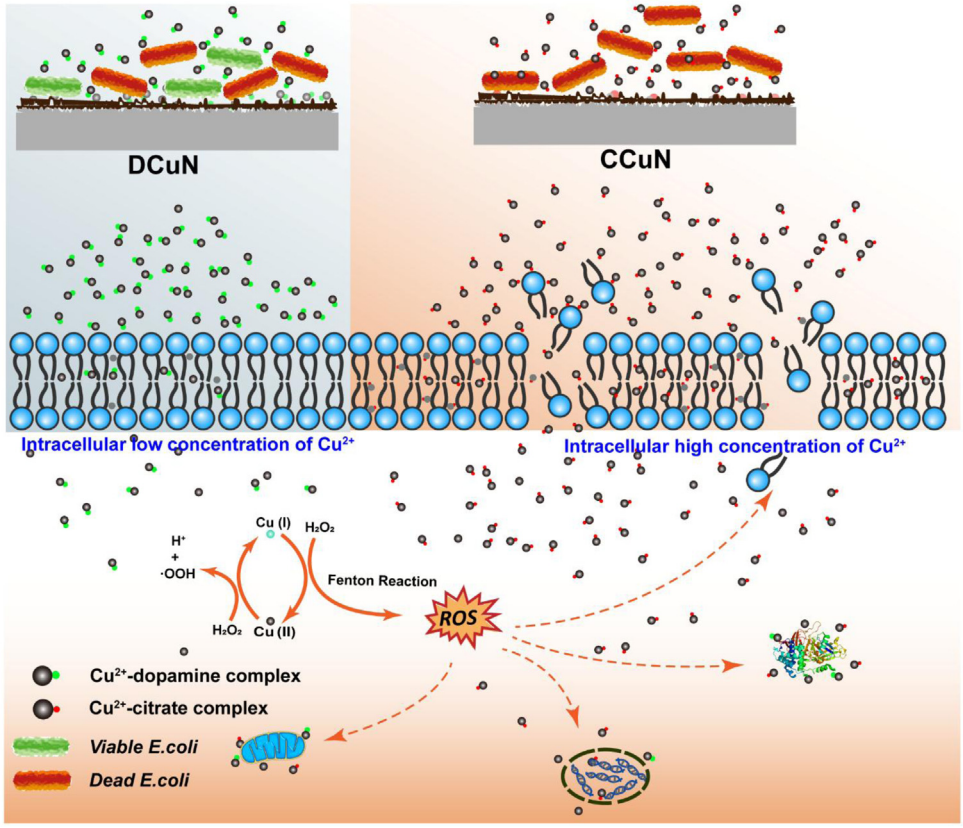

Fig. 5. Schematic illustration of bacteria-triggered synergistic bactericidal mechanism of copper-citrate nanoclusters contained porous surface.

3.3. Adhesion, proliferation, and osteodifferentiation of Ad-MSCs on CCuN samples

Introduce of copper-citrate nanoclusters into PEEK implant was expected to promote bone formation and osseointegration. Cell adhesion and proliferation are fundamental to ossification and osseointegration [38]. Therefore, cell adhesion and proliferation of Ad-MSCs were investigated. SEM and CLSM were used to observe the adhesion and morphology of cells. As detailed in Fig. 6a, cells adhered on PEEK surface exhibited narrow spreading with extended filopodia to sense the substrate after cultivating for 12 h. By contrast, on the surface of DCuN sample, cells appeared a polygonal shape with lamellipodia stretched out but barely spread filopodia. The CCuN sample had more cells attached, and the cells displayed an elongated configuration with filopodia stretched toward different directions. Consistently, cells observed by CLSM appeared poorly developed cytoskeleton (F-actin) on PEEK surface while exhibited more spreading morphology on CCuN surface (Fig. S3). Thus, these imply that CCuN sample could favor the adhesion and spreading of Ad-MSC. The existence of copper could contribute to the better performance of cell adhesion in CCuN group. However, the inconsistency of cell morphology between DCuN and CCuN group could be attributed to the increased contact angle from 37° to 56°, which would favor cell adhesion [39,40]. Cell proliferation is an event after cell adhesion [41]. Therefore, the proliferation of cells was evaluated by MTT assay. It showed that cells proliferated in a time-dependent manner during the culture period, and samples with copper, especially CCuN sample, facilitated the proliferation of cells when compared with PEEK sample (Fig. 6b). The aforementioned results suggests that CCuN samples possess better cytocompatibility than PEEK and DCuN samples, and this may lead to better osteodifferentiation performance.

To study the osteodifferentiation of Ad-MSCs cultured with different samples, a set of related evaluations were carried out. ALP activity, an early marker for osteogenic differentiation potential, was determined after cultured for 7 d. As illustrated in Fig. 6d, the ALP activity in CCuN group was the highest and compromised a bit in DCuN group, but still higher than that in PEEK group. The images of ALP staining demonstrated the same results. In Fig. 6c, the deeper the blue color, the stronger the expression of ALP. Thus, it showed clearly that CCuN group displayed the highest ALP expression and followed by DCuN and PEEK groups. To further investigate osteogenic differentiation-inducing effects of samples to Ad-MSCs, qualitative and quantitative of collagen secretion and calcium deposition were performed. Deepest red color and largest staining area for both Sirius red and ARS staining appeared in CCuN group (Fig. 6e, g), and the quantitative results were in accordance with the staining images.

Collectively, the abovementioned results suggest that the existence of copper did facilitate osteodifferentiation of Ad-MSCs. It was originated from the release of copper ions, which has been proved to promote cell proliferation and differentiation at relative low concentration (0.1 mM/6.4 μg/mL) [12]. The release amount of Cu^{2+} from DCuN and CCuN samples at physiological environment for 28 d were just under 1 μg/mL, and it would be even lower when cultured with cells because of the barrier effect of extracellular matrix (ECM) [42]. Therefore, it is evident that the released amount of Cu^{2+} at physiological environment would not undermine the activity of Ad-MSCs and conversely would promote cell differentiation. Besides that, it is noteworthy that CCuN sample exhibited higher osteodifferentiation potential than DCuN sample. The presence of citrate could be the reason. It was found that citrate can enter mesenchymal stem cells (MSCs) through a kind of membrane transporter to regulate cell energy metabolism, elevating cellular energy levels, which in turn facilitate osteophenotype progression

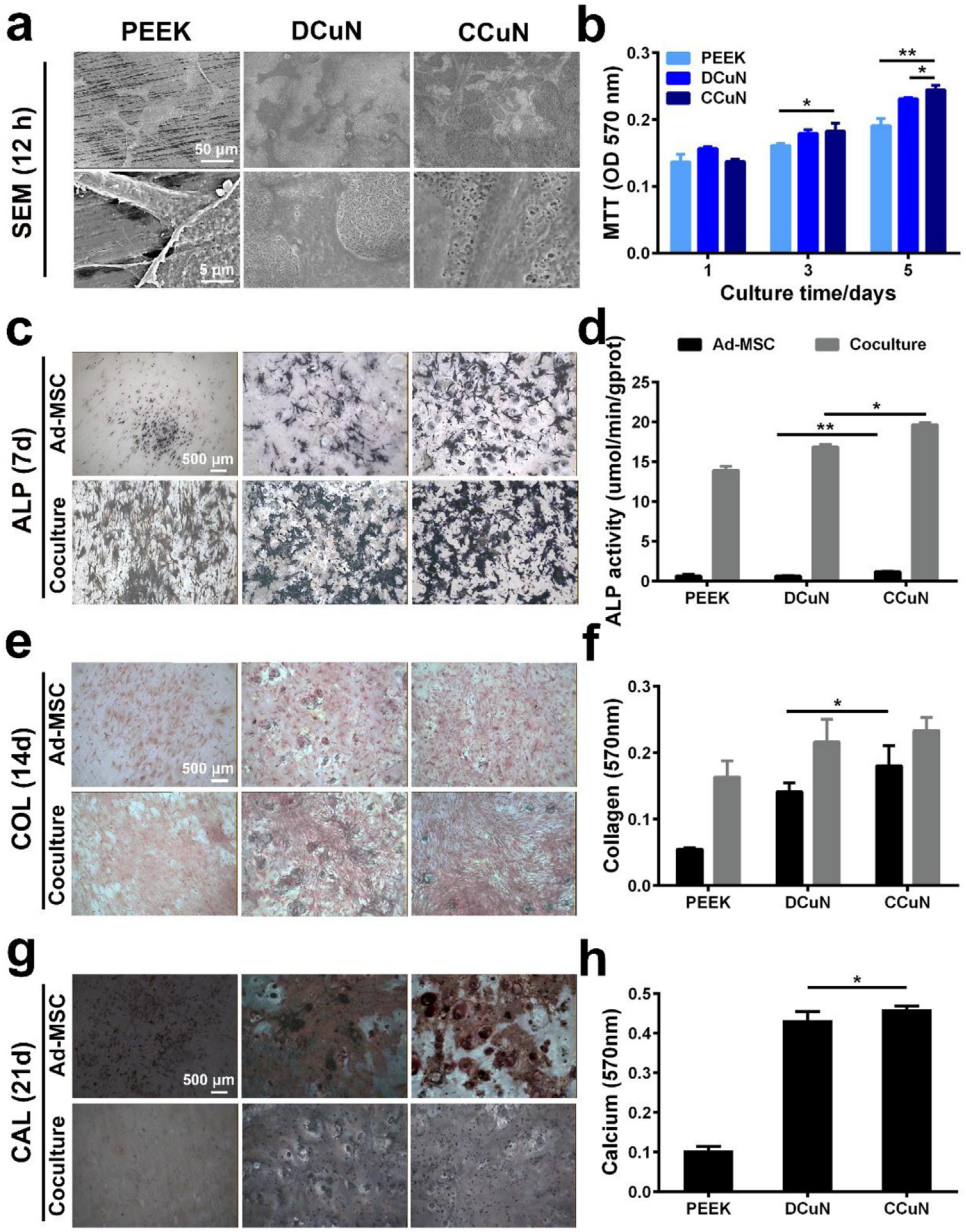

Fig. 6. *In vitro* proliferation of Ad-MSCs. (a) SEM morphology of Ad-MSCs and (b) cell activity evaluated by MTT. Osteodifferentiation of Ad-MSCs in monoculture or coculture system: (c, e, g) Qualitative and (d, f, h) quantitative of ALP expression, collagen secretion, and calcium deposition, respectively. $^{*}P < 0.05$; $^{**}P < 0.01$.

[43]. Accordingly, the application of citrate was documented to elevate ALP activity [44], increase calcium nodule formation [45], and enhance bone density [46]. Together, these results indicate the copper-citrate nanoclusters could qualify CCuN samples with enhanced osteodifferentiation ability.

3.4. Adhesion, proliferation, and vascularization of HUVECs on CCuN samples

Cortical bone is enmeshed by capillaries that interact with a network of intracortical canals consisting of longitudinal Haversian canals and transversal Volkmann canals that link the periosteum and the endosteum [47]. Thus, it would be easier to perceive the importance of adequate blood supply for bone formation, which can transport minerals, oxygen and nutrients essential for maintaining proper osteoblastic bone matrix synthesis and mineralization [48]. Angiogenesis, the formation of new capillaries from existing vasculature, involves migration and proliferation of endothelial cells and subsequent differentiation into mature blood vessels [49]. Therefore, we assessed the adhesion, proliferation, and NO production of HUVECs. SEM images showed HUVECs in PEEK group displayed a spherical shape with few filopodia stretching out while flat morphology with lamellipodia outstretching appeared for the counterparts in DCuN and CCuN groups (Fig. 7a), indicating copper is beneficial to HUVECs adhesion. The following proliferation process was assessed by MTT assay. At day 1, cells in PEEK group showed the highest activity, whereas DCuN and CCuN groups caught up and presented superior cell activity than PEEK group at day 3 (Fig. 7b). Copper, which was believed to activate an extracellular target (perhaps pro-angiogenic cytokine) to initiate angiogenesis [50], may contribute to these results. Besides, copper has been reported to strengthen the hypoxic stimulus by stabilizing the structure of hypoxia inducible factor-1α (HIF-1α), in turn inducing the transcription of vascular endothelial growth factor

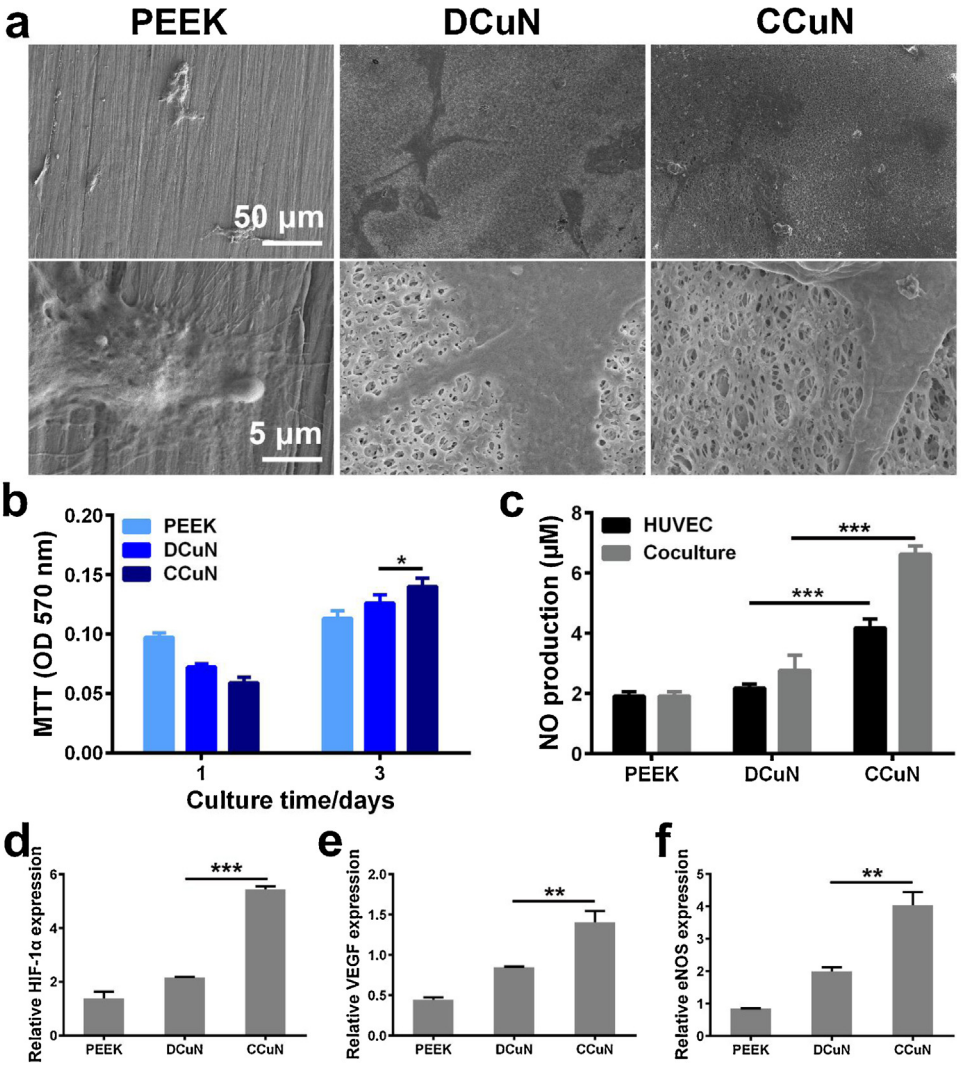

Fig. 7. *In vitro* proliferation of HUVECs. (a) SEM observation of HUVECs and (b) cell activity evaluated by MTT. (c) NO production of HUVECs in monoculture and coculture system. Gene expression of (d) HIF-1α, (e) VEGF, and (f) eNOS. $^{*}P < 0.05$; $^{**}P < 0.01$; $^{***}P < 0.001$.

(VEGF), activating endothelial nitric oxide synthase (eNOS), and increasing the release of nitric oxide (NO) [19,51], eventually leading to angiogenesis [52]. Thereby, the production of NO and the expression of relative genes were measured. The expression of HIF-1α, which is directly associated with the concentration of copper, was enhanced by the stimulation of copper containing-samples. In detail, CCuN samples upregulated 2-fold expression of HIF-1α compared with DCuN sample (Fig. 7d). This may associated with the result that citrate potentiated the influx of copper into cells by 2 times compared with copper alone. Then theoretically, the expression of HIF-1α would activate the transcription of VEGF, which is a key regulator of angiogenesis [53]. Accordingly, our results showed that VEGF was mainly expressed in CCuN group and compromised in DCuN group (Fig. 7e). Its downstream factor eNOS, which directly relates to the production of NO, shared the same trend in expression with the production of NO in different groups. Specifically, as depicted in Fig. 7c, f, the expression of eNOS and production of NO were elevated in DCuN group compared with the counterpart in PEEK group, whereas a 2-fold increase of eNOS expression and NO production were achieved in CCuN group compared with DCuN group. These results clearly reveal that CCuN possesses stronger ability of promoting angiogenesis than DCuN. The ability of citrate to potentiate the influx of copper into cells by 2 times compared with copper alone may be the reason, as angiogenesis capacity is associated with intracellular copper levels [54,55]. Additionally, citrate also has been reported to be able to promote angiogenesis [22]. These together endow better angiogenesis capacity to CCuN.

3.5. Osteodifferentiation and angiogenesis in coculture system

To further investigate the osteogenic and angiogenic ability of samples, a cocuture system was used. It is more closely represent the real situation of tissue regeneration than the monoculture system. All of these results, except calcium deposition, from coculture system shared the same trend with the results from monoculture system, which was that CCuN samples possess the highest osteodifferentiation and angiogenesis abilities followed by DCuN and PEEK samples. What's interesting, the coculture system per se, which allows the fully crosstalk between Ad-MSCs and HUVECs, exerted positive effects on the early differentiation of Ad-MSCs, whereas inhibited their later mineralization. The staining images of ALP expression and collagen secretion in coculture system demonstrated enhanced osteogenic potential of Ad-MSCs compared with monoculture of Ad-MSCs (Fig. 6c, e). Consistently, the quantitative of ALP activity and collagen secretion revealed the same trend, and notably, it exhibited a 20-fold increase of ALP activity in coculture system compared with monoculture (Fig. 6d, f). However, no

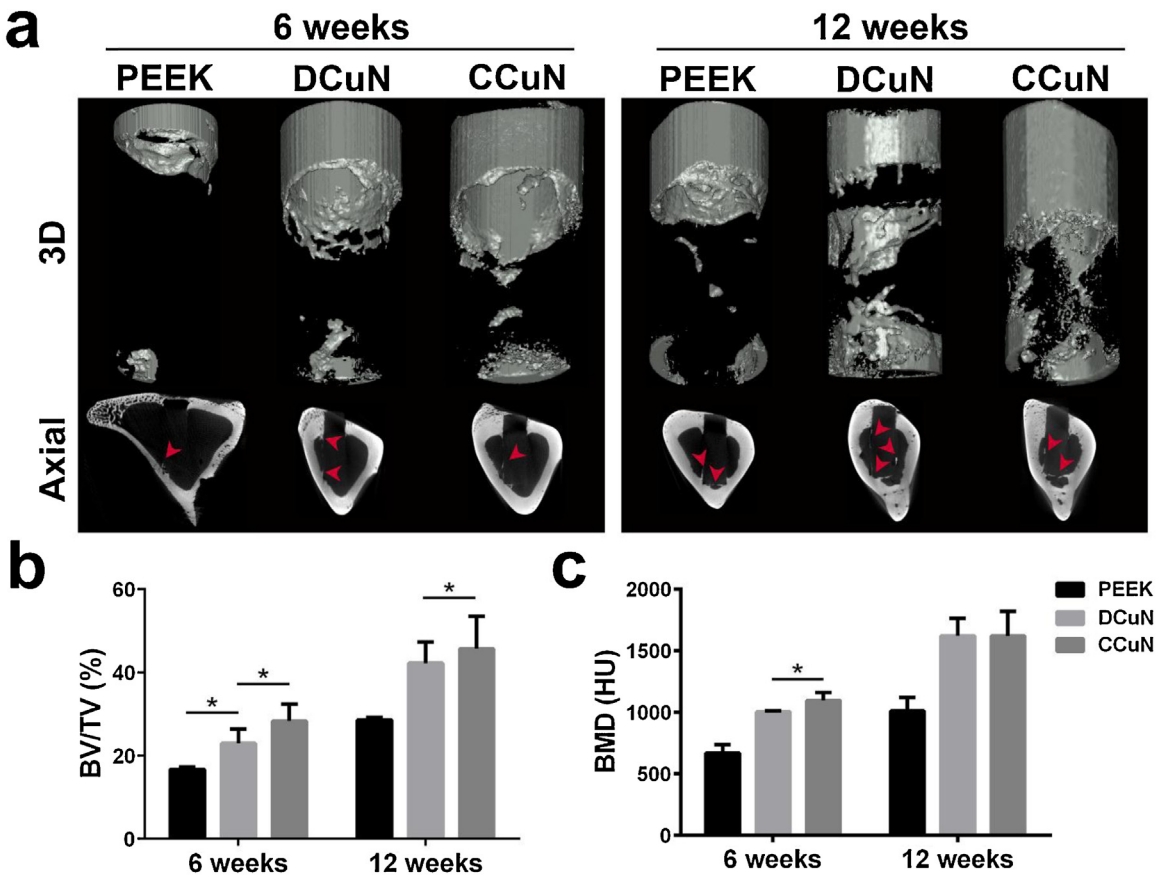

Fig. 8. Micro-CT imaging and quantification of bone regeneration. (a) 3D reconstructed micro-CT images of the new bone formation and corresponding micro-CT images of the tibia bone defect in the axial plane at 6, and 12 weeks after implantation. Quantitative histomorphometry analyses of (b) BV/TV and (c) BMD. $^{*}P < 0.05$.

calcium deposition occurred on the surface of samples in the coculture system (Fig. 6g), indicating coculture with HUVECs abolished the mineralization ability of Ad-MSCs. The inhibitory effect on the later mineralization has been disclosed and it is originated from the suppression of osterix (OSX) expression, so as to arrest Ad-MSCs differentiation at a pre-osteoblastic stage, avoiding mineral deposition within vessels [56].

On the other hand, it is widely accepted that the crosstalk between ECs and MSCs advances angiogenesis [57], which is accordance with our results. NO is regarded as a mediator of angiogenesis [51], and the coculture system facilitated the production of NO especially in CCuN group (Fig. 7c).

Collectively, these results point out that CCuN samples still maintain their ability to potentiate the osteogenesis and angiogenesis in coculture system, and it is noteworthy that the coculture system per se elicits different effects on osteogenesis and angiogenesis.

3.6. In vivo *studies*

To examine the osteogenesis and osseointegration performances of implants with constructed coating, an established rabbit tibia model was used. Micro-CT was employed to evaluate the osteogenic capability. Bone formation was observed on the 3D remodeling images and axial images, and these images presented that CCuN group possessed the highest new bone volume at both 6 and 12 weeks (Fig. 8a). Consistently, at 6 weeks, quantitative results displayed the highest BV/TV in CCuN group and compromised in DCuN group which was still significantly higher than the counterpart of PEEK group. At 12 weeks, the BV/TV values of all groups kept the same trend as at 6 weeks but all increased (Fig. 8b). Additionally, the copper containing group increased the BMD and the involvement of citrate further improved it (Fig. 8c). It is clear that CCuN implants are beneficial to bone regeneration and accelerate bone formation compared with both DCuN and PEEK implants. The integration between bone and implants was evaluated by methylene blue and acid fuchsine staining of hard tissue slices and SEM observation of hard tissue slices. At week 6, a thick layer of fibrous connective tissue was shown to separate the bone tissue from PEEK implants, while which was much thinner and discontinuous between DCuN implants and bone tissue. For CCuN implants, it exhibited tighter integration and new bone appeared inside some of the pore structure. After implantation for 12 weeks, the fibrous connective tissue was gradually replaced by newly formed bone, leading to reduced gap between implants and bone tissue. However, there was still a thin layer of fibrous connective tissue around PEEK implants, whereas CCuN implants performed a complete osseointegration (Fig. 9). The SEM observation and elemental mappings further proved this results (Fig. S4). It showed that a layer full of carbon, which is fibrous connective tissue, separated PEEK/DCuN implants from bone tissue at week 6, and no sign of fibrous connective tissue appeared between the CCuN implants and bone tissue. At week 12, the fibrous connective tissue layer became thinner in PEEK group and disappeared in DCuN group. As to CCuN group, the calcium distribution indicated the appearance of bone tissue inside the porous structure of CCuN implants.

Collectively, these results demonstrate that CCuN implants possess better performances in bone regeneration and osseointegration compared with DCuN and PEEK implants. The existence of

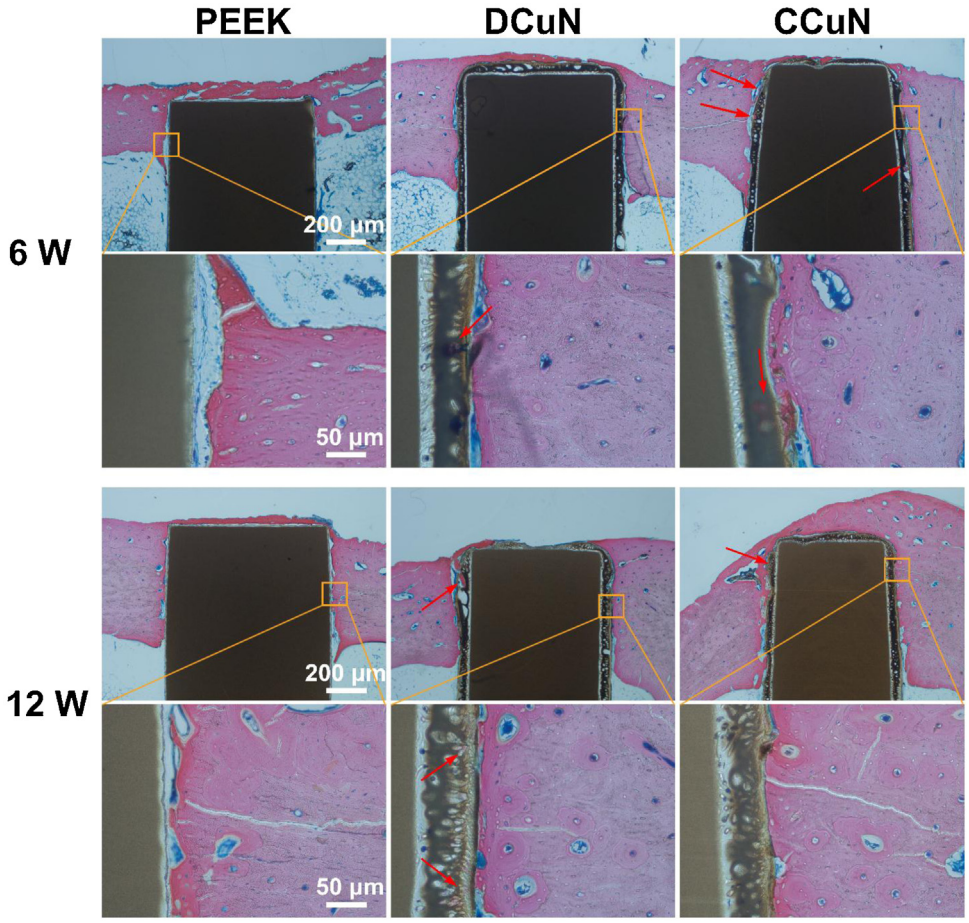

Fig. 9. The methylene blue and acid fuchsine staining in each group at 6 and 12 weeks post-surgery.

copper definitely has a contribution to it because of its well-known bone regeneration property [9]. Nevertheless, its combination with citrate should be the factor that makes CCuN implants stand out in successful implantation when compared with DCuN implants. Citrate can not only promote osteogenesis through regulating cellular behavior, which has been elaborated above, but also can advance bone regeneration by facilitating the deposition of calcium phosphate. It was found that citrate molecules makes up about 5 wt% of the total organic component in bone and that over 90 % of the body's total citrate content is located in the skeletal system [58]. The existence of citrate can regulate bone generation not only through improving the wetting effect at the collagen-mineral interface [59], but also through stabilizing bone apatite and controlling the size and crystallinity of hydroxyapatite (HA) particles [60–62]. Thus, it is fully understandable that CCuN implants performed the most satisfying results *in vivo*.

4. Conclusion

In the field of orthopedic implantation, the major difficulty is to achieve a rapid bone regeneration and a stable bone-implant integration, particularly when faced with implant-associated infection. Therefore, PEEK implant coated with polydopamine based copper-citrate nanoclusters was developed. The *in vitro* studies showed promoted osteodifferentiation and angiogenesis, as well as enhanced bacteria-triggered bacteria-killing performance in CCuN group due to the synergistic effect between copper and citrate, while the *in vivo* studies displayed enhanced bone regeneration and integration in CCuN implants. This triplet functional implant can guarantee the success of implantation, and the excellent flexibility of coating construction procedure suggests it is applicable to different medical devices even with complicated shapes and architectures.

Declaration of Competing Interest

The authors declare no potential conflict of interest.

Acknowledgments

This work was financially supported by the National Key Research and Development Project (2018YFC1106600), National Natural Science Foundation of China (No. 31670974, No. 31370954, No. 51901003).

References

[1] S.M. Kurtz, J.N. Devine, Biomaterials 28 (2007) 4845–4869.
[2] A. Dong, Y.J. Wang, Y. Gao, T. Gao, G. Gao, Chem. Rev. 117 (2017) 4806–4862.
[3] J. Liang, H. Wang, M. Libera, Biomaterials 204 (2019) 25–35.
[4] Y. Zhang, P. Sun, L. Zhang, Z. Wang, F. Wang, K. Dong, Z. Liu, J. Ren, X. Qu, Adv. Funct. Mater. 29 (2019).
[5] S. Jiang, Z. Cao, Adv. Mater. 22 (2010) 920–932.
[6] J. Min, K.Y. Choi, E.C. Dreaden, R.F. Padera, R.D. Braatz, M. Spector, P.T. Hammond, ACS Nano 10 (2016) 4441–4450.
[7] J. Yan, W. Zhou, Z. Jia, P. Xiong, Y. Li, P. Wang, Q. Li, Y. Cheng, Y. Zheng, Acta Biomater. 79 (2018) 216–229.
[8] W. Liu, J. Li, M. Cheng, Q. Wang, Y. Qian, K.W.K. Yeung, P.K. Chu, X. Zhang, Biomaterials 208 (2019) 8–20.
[9] E.J. Ryan, A.J. Ryan, A. Gonzalez-Vazquez, A. Philippart, F.E. Ciraldo, C. Hobbs, V. Nicolosi, A.R. Boccaccini, C.J. Kearney, F.J. O'Brien, Biomaterials 197 (2019) 405–416.

[10] C. Prinz, M. Elhensheri, J. Rychly, H.-G. Neumann, J. Biomater. Appl. 32 (2017) 139–149.
[11] W.-L. Du, S.-S. Niu, Y.-L. Xu, Z.-R. Xu, C.-L. Fan, Carbohydr. Polym. 75 (2009) 385–389.
[12] I. Burghardt, F. Luthen, C. Prinz, B. Kreikemeyer, C. Zietz, H.G. Neumann, J. Rychly, Biomaterials 44 (2015) 36–44.
[13] R.T. Tran, J. Yang, G.A. Ameer, Annu. Rev. Mater. Res. 45 (2015) 277–310.
[14] L.C. Su, Z. Xie, Y. Zhang, K.T. Nguyen, J. Yang, Front. Bioeng. Biotechnol. 2 (2014) 23.
[15] J.A. Lemire, J.J. Harrison, R.J. Turner, Nat. Rev. Microbiol. 11 (2013) 371–384.
[16] Y. Liu, K. Ai, L. Lu, Chem. Rev. 114 (2014) 5057–5115.
[17] Y. Yu, G. Jin, Y. Xue, D. Wang, X. Liu, J. Sun, Acta Biomater. 49 (2017) 590–603.
[18] D. Zou, Z. Zhang, J. He, K. Zhang, D. Ye, W. Han, J. Zhou, Y. Wang, Q. Li, X. Liu, X. Zhang, S. Wang, J. Hu, C. Zhu, W. Zhang, Y. zhou, H. Fu, Y. Huang, X. Jiang, Biomaterials 33 (2012) 2097–2108.
[19] E. Urso, M. Maffia, J. Vasc. Res. 52 (2015) 172–196.
[20] L. Zentilin, S. Tafuro, S. Zacchigna, N. Arsic, L. Pattarini, M. Sinigaglia, M. Giacca, Blood 107 (2006) 3546–3554.
[21] Y. Wang, M. Nakayama, M.E. Pitulescu, T.S. Schmidt, M.L. Bochenek, A. Sakakibara, S. Adams, A. Davy, U. Deutsch, U. Luthi, A. Barberis, L.E. Benjamin, T. Makinen, C.D. Nobes, R.H. Adams, Nature 465 (2010) 483–486.
[22] S. Binu, S.J. Soumya, P.R. Sudhakaran, J. Physiol. Biochem. 69 (2013) 383–395.
[23] S.K. Ramasamy, A.P. Kusumbe, L. Wang, R.H. Adams, Nature 507 (2014) 376–380.
[24] Y. Zhao, H.M. Wong, W. Wang, P. Li, Z. Xu, E.Y. Chong, C.H. Yan, K.W. Yeung, P.K. Chu, Biomaterials 34 (2013) 9264–9277.
[25] M.H. Ryou, Y.M. Lee, J.K. Park, J.W. Choi, Adv. Mater. 23 (2011) 3066–3070.
[26] D.R. Dreyer, D.J. Miller, B.D. Freeman, D.R. Paul, C.W. Bielawski, Langmuir 28 (2012) 6428–6435.
[27] A.V. Tran, K. Shim, T.T. Vo Thi, J.K. Kook, S.S.A. An, S.W. Lee, Acta Biomater. 74 (2018) 397–413.
[28] R. Sánchez-Clemente, M.I. Igeño, A.G. Población, M.I. Guijo, F. Merchán, R. Blasco, Proceedings 2 (2018).
[29] E. Seebach, K.F. Kubatzky, Front. Immunol. 10 (2019) 1724.
[30] K.Y. Djoko, M.D. Phan, K.M. Peters, M.J. Walker, M.A. Schembri, A.G. McEwan, Proc. Natl. Acad. Sci. U. S. A. 114 (2017) 6818–6823.
[31] E.I. Koh, A.E. Robinson, N. Bandara, B.E. Rogers, J.P. Henderson, Nat. Chem. Biol. 13 (2017) 1016–1021.
[32] J.C. Wilks, J.L. Slonczewski, J. Bacteriol. 189 (2007) 5601–5607.
[33] D. Zhitnitsky, J. Rose, O. Lewinson, Sci. Rep. 7 (2017) 44554.
[34] M. Valko, H. Morris, M. Cronin, Curr. Med. Chem. 12 (2005) 1161–1208.
[35] L. Macomber, C. Rensing, J.A. Imlay, J. Bacteriol. 189 (2007) 1616–1626.
[36] J.A. Imlay, Annu. Rev. Microbiol. 57 (2003) 395–418.
[37] L. Macomber, J.A. Imlay, Proc. Natl. Acad. Sci. U. S. A. 106 (2009) 8344–8349.
[38] A. Chug, S. Shukla, L. Mahesh, S. Jadwani, J. Oral Maxillofac. Surg. Med. Pathol. 25 (2013) 1–4.
[39] L.C. Xu, C.A. Siedlecki, Biomaterials 28 (2007) 3273–3283.
[40] C.C. Barrias, M.C. Martins, G. Almeida-Porada, M.A. Barbosa, P.L. Granja, Biomaterials 30 (2009) 307–316.
[41] Z. Luo, J. Pan, Y. Sun, S. Zhang, Y. Yang, H. Liu, Y. Li, X. Xu, Y. Sui, S. Wei, Adv. Funct. Mater. 28 (2018).
[42] Z. Jia, P. Xiu, M. Li, X. Xu, Y. Shi, Y. Cheng, S. Wei, Y. Zheng, T. Xi, H. Cai, Z. Liu, Biomaterials 75 (2016) 203–222.
[43] C. Ma, X. Tian, J.P. Kim, D. Xie, X. Ao, D. Shan, Q. Lin, M.R. Hudock, X. Bai, J. Yang, Proc. Natl. Acad. Sci. U. S. A. 115 (2018) E11741–E11750.
[44] R.T. Tran, L. Wang, C. Zhang, M. Huang, W. Tang, C. Zhang, Z. Zhang, D. Jin, B. Banik, J.L. Brown, Z. Xie, X. Bai, J. Yang, J. Biomed. Mater. Res. A. 102 (2014) 2521–2532.
[45] D. Gyawali, P. Nair, H.K. Kim, J. Yang, Biomater. Sci. 1 (2013) 52–64.
[46] S. Jehle, H.N. Hulter, R. Krapf, J. Clin, Endocrinol. Metab. Seoul (Seoul) 98 (2013) 207–217.
[47] H. Xie, Z. Cui, L. Wang, Z. Xia, Y. Hu, L. Xian, C. Li, L. Xie, J. Crane, M. Wan, G. Zhen, Q. Bian, B. Yu, W. Chang, T. Qiu, M. Pickarski, L.T. Duong, J.J. Windle, X. Luo, E. Liao, X. Cao, Nat. Med. 20 (2014) 1270–1278.
[48] C.J. Percival, J.T. Richtsmeier, Dev. Dyn. 242 (2013) 909–922.
[49] S. Liekens, E. De Clercq, J. Neyts, Biochem. Pharmacol. 61 (2001) 253–270.
[50] L. Finney, S. Mandava, L. Ursos, W. Zhang, D. Rodi, S. Vogt, D. Legnini, J. Maser, F. Ikpatt, O.I. Olopade, D. Glesne, Proc. Natl. Acad. Sci. U. S. A. 104 (2007) 2247–2252.
[51] J.P. Cooke, D.W. Losordo, Circulation 105 (2002) 2133–2135.
[52] C. Coletta, A. Papapetropoulos, K. Erdelyi, G. Olah, K. Modis, P. Panopoulos, A. Asimakopoulou, D. Gero, I. Sharina, E. Martin, C. Szabo, Proc. Natl. Acad. Sci. U. S. A. 109 (2012) 9161–9166.
[53] N. Ferrara, H.P. Gerber, J. LeCouter, Nat. Med. 9 (2003) 669–676.
[54] L. Finney, S. Vogt, T. Fukai, D. Glesne, Clin. Exp. Pharmacol. Physiol. 36 (2009) 88–94.
[55] G. Narayanan, B.S. R, H. Vuyyuru, B. Muthuvel, S. Konerirajapuram Natrajan,PLoS One 8 (2013), e71982.
[56] T. Meury, S. Verrier, M. Alini, J. Cell, Biochem. 98 (2006) 992–1006.
[57] B.M. Beckermann, G. Kallifatidis, A. Groth, D. Frommhold, A. Apel, J. Mattern, A.V. Salnikov, G. Moldenhauer, W. Wagner, A. Diehlmann, R. Saffrich, M. Schubert, A.D. Ho, N. Giese, M.W. Buchler, H. Friess, P. Buchler, I. Herr, Br. J. Cancer 99 (2008) 622–631.
[58] C. Ma, E. Gerhard, D. Lu, J. Yang, Biomaterials 178 (2018) 383–400.
[59] C. Shao, R. Zhao, S. Jiang, S. Yao, Z. Wu, B. Jin, Y. Yang, H. Pan, R. Tang, Adv. Mater. 30 (2018).
[60] Y.Y. Hu, A. Rawal, K. Schmidt-Rohr, Proc. Natl. Acad. Sci. U. S. A. 107 (2010) 22425–22429.
[61] Y.Y. Hu, X.P. Liu, X. Ma, A. Rawal, T. Prozorov, M. Akinc, S.K. Mallapragada, K. Schmidt-Rohr, Chem. Mater. 23 (2011) 2481–2490.
[62] E. Davies, K.H. Muller, W.C. Wong, C.J. Pickard, D.G. Reid, J.N. Skepper, M.J. Duer, Proc. Natl. Acad. Sci. U. S. A. 111 (2014) E1354–63.